Journal of Materials Chemistry A

Accepted Manuscript

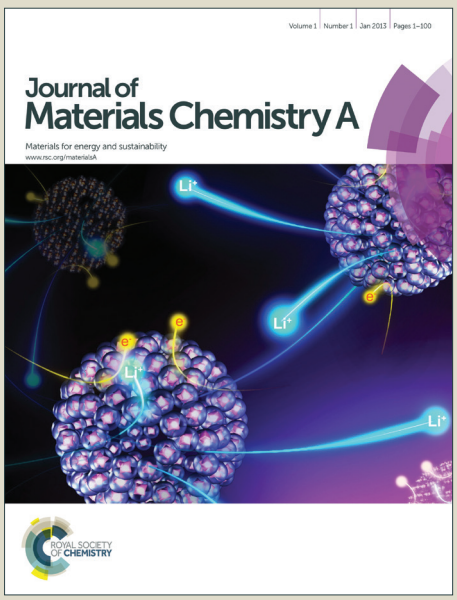

ROYAL SOCIETY OF CHEMISTRY

www.rsc.org/materialsA

Journal Name

ARTICLE

Hydraulic Power and Electric Field Combined Antifouling Effect of Novel Conductive Poly(aminoanthraquinone)/Reduced Graphene Oxide Nanohybrid Blended PVDF Ultrafiltration Membrane

Received 00th January 20xx,
Accepted 00th January 20xx

DOI: 10.1039/x0xx00000x

www.rsc.org/

Haiyan Liu,[a] Guoquan Zhang,*[a] Chuanqi Zhao,[a] Jiadong Liu,[b] Fenglin Yang[a]

Membrane fouling is still a bottleneck problem towards the wide-spread applications of membrane bioreactors (MBRs) for wastewater treatment/reclamation. Thus, membrane modification has ever been a hot topic for improving separation efficiency and antifouling ability of membrane. In this study, a novel conductive and hydrophilic poly(1,5-diaminoanthraquinone)/reduced graphene oxide (PDAAQ/rGO) nanohybrid blended polyvinylidene fluoride (PVDF) membrane was prepared by phase inversion method. The fabricated PDAAQ/rGO/PVDF membrane was characterized by different characterization techniques. The effect of additives content on membrane structure and antifouling performance was evaluated. An obvious growth in pore size/porosity and surface roughness was observed for 1.5 wt% PDAAQ/rGO naohybrid blended membrane, which caused higher hydrophilicity, pure water flux and fouling resistance than those of the pristine PVDF membrane. By applying an appropriate external electric field of 1.0 V/cm, the conductive PDAAQ/rGO nanohybrid blended PVDF membrane exhibited an admirable electrocatalytic activity towards oxygen reduction reaction, and 8.84 mg L^{-1} H_2O_2 was accumulated within 30 min electrolysis. In the meanwhile, the conductive PDAAQ/rGO/PVDF membrane displayed superior fouling removal ability along with higher water flux recovery ratio after the electric cleaning. Applying bovine serum albumin as model protein and 1.0 V/cm external electric field, the fouling rate of conductive PDAAQ/rGO/PVDF membrane was decreased by about 63.5% when compared with the control test during long-term continuous-flow membrane filtration process. The cross-flow shear stress induced by aeration scouring and the increased electrostatic repulsion force induced by external electric field and the in-situ electro-generated H_2O_2 contributed to the prominent fouling mitigation and fouling resistance.

1. Introduction

Polyvinylidene fluoride (PVDF), which can form asymmetric membrane structure by a simple immersion precipitation process, has been extensively used in microfiltration (MF) and ultrafiltration (UF) technologies with regard to its significant advantages such as good mechanical and film forming properties, strong thermal and hydrolytic stabilities as well as excellent corrosion resistance to most chemicals and organic compounds.[1-3] However, it is widely accepted that membranes with rough surfaces, high hydrophobicity and large pore sizes suffer from high permeate loss and heavy irreversible fouling during water treatment processes.[1] The strong hydrophobic surface of the pristine PVDF membranes is thus susceptible to fouling while treating aqueous solution containing natural organic and colloidal matters, e.g. proteins, which are prone to deposition and absorption onto membrane surface or blocking surface pore, resulting in low water flux, high hydraulic resistance and high operation & maintenance (O&M) costs.[4,5] Therefore, many studies on PVDF membranes have been conducted to tune the surface hydrophilicity and antifouling property through the improvement of membrane preparation process and surface modification of the pristine membranes.[6]

The blending of inorganic nanoparticles to form polymer-inorganic nanoparticles composite membranes presents an interesting approach to significantly improve the hydrophilic property and fouling resistance of polymer membranes.[7] During the preparation process, the commonly used nanoparticles/naomaterials such as TiO_2,[8-11] SiO_2,[12-14] Al_2O_3,[11,15] ZnO,[16] and graphene oxide[17-23] can be facilely incorporated into PVDF membranes through blending them in coagulation bath or in polymer solution. However, the aggregation and poor adhesion of inorganic nanopractices limit the beneficial effects of the modified PVDF membrane. Additionally, the high concentration of inorganic nanopractices affects the membrane-forming process, leading to a poor

[a] Key Laboratory of Industrial Ecology and Environmental Engineering, Ministry of Education, School of Environmental Science and Technology, Dalian University of Technology, Dalian 116024, China. E-mail: guoquanz@126.com (G. Zhang)
[b] Key Laboratory of Northwest Water Resources and Ecological Environment, Ministry of Education, School of Environmental and Municipal Engineering, Xi'an University of Architecture & Technology, Xi'an 710055, China

mechanical stability.[1] The blending of hydrophilic polymers such as polyvinyl alcohol (PVA),[8,24] polyethylene glycol (PEG) derivatives[25,26] and polyvinyl pyrrolidone (PVP)[27,28] is another simple way to enhance the hydrophilicity of PVDF membranes during the phase separation process. Unfortunately, the poor compatibility of hydrophilic polymers with hydrophobic PVDF matrix leads to the formation of interface microvoid, resulting in worse physical and mechanical properties compared to those of the pristine PVDF membranes, which is disadvantageous to the practical applications.[1,24]

In general, membrane fouling of membrane bioreactors (MBRs) is attributed mainly to the adsorption/deposition of particulate and soluble materials including negatively charged sludge flocs, soluble microbial products (SMP) and extracellular polymeric substances (EPS) on membrane surfaces and/or into membrane pores.[29,30] Therefore, a negatively charged membrane surface by introducing an external electric field can efficiently increase the electrostatic repulsive force between membranes and fouling agents, suppressing both pore blocking and surface gel formation.[29-36] Apart from the conductive metal oxide nanoparticles, the traditional conducting polymers, such as polypyrrole, have been used as the potential current-carrying materials to optimize filtration membranes.[36-38] Nevertheless, these polymers are difficult to be flexibly processed as done with most other plastic products. As a result, the final membranes made from these materials suffer from low flux, poor separation performances, brittleness, and often, low conductivity.[37] Alternatively, the low dimensional carbon nanomaterials like carbon nanotubes (CNTs)[18,31,39-42] and reduced graphene oxide (rGO)[18,43] were also adopted as nano-fillers in polymer composite membranes to overcome the limitation of innate insulating nature of polymers and to tune surface charges and hydrophilcity. More recently, great efforts have also been made to directly utilize the highly electrically conductive polymer nanocomposite blended membranes as cathodes, which has been proved as a simple but efficacious manner for decreasing fouling and increasing permeate flux in MBRs.[44,45] In these researches, besides the electrostatic repulsive function, the adsorbed/deposited foulants on membrane surface and/or in circuitous nanochannels can also be decomposed quickly under the action of external electric field when endowing these conductive membranes with electrocatalytic properties, thus achieving the on-line self-cleaning function of these filtration membranes. Our previous studies have investigated the electrochemical and electrocatalytic performance of poly(1,5-diaminoanthraquinone)/reduced graphene oxide (PDAAQ/rGO) nanohybrid that is synthesized by a one-step potentiodynamic deposition method.[46] The PDAAQ/rGO nanohybrid exhibited high conductivity, porosity and superior electrocatalytic activity towards oxygen reduction reaction (ORR) with a long cycle life. To date, exploiting conductive polymer nanocomposite blended membranes and mitigating their fouling by an external electric field is very scarce, and the antifouling property as well as electric cleaning mechanism of PDAAQ/rGO nanohybrid blended PVDF membranes has not been investigated yet in MBRs.

Herein, a novel conductive PDAAQ/rGO/PVDF membrane was prepared by phase inversion method using PDAAQ/rGO nanohybrid as functional fillers and PVDF as the polymer host, which can be directly used as both cathode and separation membrane. The effects of additives type and content on the membrane hydrophilicity, water permeability and bovine serum albumin (BSA) rejection were investigated in detail. The fouling mitigation and antifouling ability of conductive PDAAQ/rGO/PVDF membrane were investigated with an external electric field in electric cleaning and long-term continuous-flow membrane filtration processes. Results indicate that the PDAAQ/rGO/PVDF blending membranes possess excellent antifouling function under an appropriate external voltage, which can effectively reduce membrane fouling and improve filtration efficiency under the actions of cross-flow shear stress and electrostatic repulsive force, achieving the on-line hydraulic power and electric field combined antifouling effect.

2. Experimental

2.1 Materials

Natural flake graphite powder (600 mesh, 99.99%) was purchased from Sinopharm Chemical Reagent Co., Ltd. PVDF (FR904, $M_w = 2 \times 10^6$, $M_n = 4.7 \times 10^5$) was obtained from Shanghai 3F New Materials Co., Ltd. Analytical grade 1,5-diaminoanthraquinone (DAAQ) monomer, ethanol, N,N-dimethylformamide (DMF), CrO_3, H_2SO_4 (98%), L-Ascorbic acid (LAA) and chromatographic grade bovine serum albumin (BSA, MW = 68 kDa) was supplied by Beijing Solarbio Science & Technology Co., Ltd. and were used without further purification. Distilled water was used for all experiments.

2.2 Synthesis of PDAAQ/rGO nanohybrid

Graphene oxide (GO) nanosheets were synthesized by the chemical oxidation of natural flake graphite using a modified Hummers method.[47] The PDAAQ/rGO nanohybrids were prepared by a two-step process, i.e. oxidative polymerization and reduction. Typically, 100 mg GO nanosheets were added into a 500 mL conical flask containing 100 mL DMF and 1 mol L^{-1} H_2SO_4 to form a stable suspension via ultrasonication for 2 h. Then, 233 mg 1,5-DAAQ monomer was dissolved in this mixture solution by ultrasonication for 1 h, resulting in a monomer solution with an optimal mass ratio between 1,5-DAAQ and GO of 7:3 (w/w), as reported previously.[46] According to a total molar ratio of 1,5-DAAQ monomer to oxidant of 3:1, approximately 33 mg chromium trioxide (CrO_3) was dissolved separately in 100 ml DMF and 1 mol L^{-1} H_2SO_4 to form the oxidant solution. Subsequently, the oxidant solution was added drop-wise into the monomer solution in a 20 °C water bath for 4 h, and the reaction mixture was magnetically stirred for 24 h followed by vacuum filtration before being washed with excess DMF and distilled water to remove the oligomers, monomer and oxidant. The collected polymer particles were dispersed in 300 mL distilled water to form a uniform dispersion by ultrasonication. Then, 1.0 g L-ascorbic acid (L-AA, vitamin C) which acted as the reducing agent was

dissolved into this uniform dispersion by ultrasonication for 2 h and this mixture was kept at room temperature for a further 24 h. The compound was washed with excess distilled water and dried in a vacuum oven at 60 °C. Finally, approximately 250 mg PDAAQ/rGO nanohybrid black solid powder was obtained with a yield of approximately 75%.

2.3 Synthesis of PDAAQ/rGO/PVDF membranes

The PDAAQ/rGO nanohybrid blended PVDF membranes were prepared by the general phase inversion method with PVDF used as the bulk material, DMF as the solvent, PDAAQ/rGO nanohybrid as the additive and deionized water as the nonsolvent coagulation bath. Prior to mixing, all the samples were dried at 80 ^{0}C in a vacuum oven to remove the absorbed water. The PDAAQ/rGO nanohybrid (0.5, 1.0, 1.5 and 2.0 wt% based on the weight of PVDF) were added into DMF by ultrasonication for 6 h. PVDF (14 wt%) was dissolved in PDAAQ/rGO/DMF solution under a constant stirring rate for 24 h in a 60 ^{0}C water bath to form homogenous casting solutions. After fully degassing, the mixed solution was uniformly spread onto a glass plate and scraped to be a nascent membrane with 200 μm thickness. After exposure to air for 20 s, the nascent membrane was immersed into a 20 ^{0}C coagulation bath. After solidification, the membranes were peeled off from the glass plate and washed until the residual solvents entirely removed, and then stored in distilled water for the characterization and test. The schematic illustration about the preparation process of PDAAQ/rGO nanohybrid blended PVDF membranes is shown in **Figure 1**. Simultaneously, pristine PVDF, rGO and PDAAQ blended PVDF membranes were also prepared by the same process as a contrast.

2.4 Basic physicochemical characterizations

The surface and cross-section membrane morphologies were examined by a field emission scanning electron microscope (FE-SEM, Nova Nanosem 450, FEI Company, USA). To observe the cross-section morphology, the freeze dried membrane samples were fractured in liquid nitrogen. The chemical compositions of membranes were investigated by Fourier transform infrared (FT-IR, EQUINOX 55, Bruker Optics, German) absorption spectra in the range of 4000-400 cm^{-1} with attenuated total reflection (ATR) accessory. X-ray photoelectron spectroscopy (XPS) was used to investigate the surface chemical compositions of samples, which was conducted on an AXIS Ultra DLD spectrometer (Shimadzu, Japan) with a monochromatized Al Ka X-ray source (1486.6 eV photons) at a constant dwell time of 250 ms and a pass energy of 40 eV. The membrane surface roughness was examined by an atomic-force microscopy (AFM, PicoScan2500 Controller, Agilent Technologies formerly Molecular Imaging, Corp, USA) equipped with a 5 × 5 mm scanner using tapping mode of a silicon nitride AFM probe (Ted Pella Inc, USA) at room temperature. The membranes hydrophilicity was evaluated by contact angle measuring on a Drop Shape Analysis system (DSA100, Kruss Company, Germany). The electrocatalytic activities of the pristine PVDF, rGO, PDAAQ and PDAAQ/rGO blending PVDF membranes (area of 4 cm^2) were investigated by cyclic voltammetry (CV) technique with a PARC model 263A potentiostat/galvanostat. A Pt sheet (0.81 cm^2) and 1M Ag/AgCl were used as the counter and the standard reference electrodes, respectively. All electrolytes were prepared with ultrapure water (>18 MΩ).

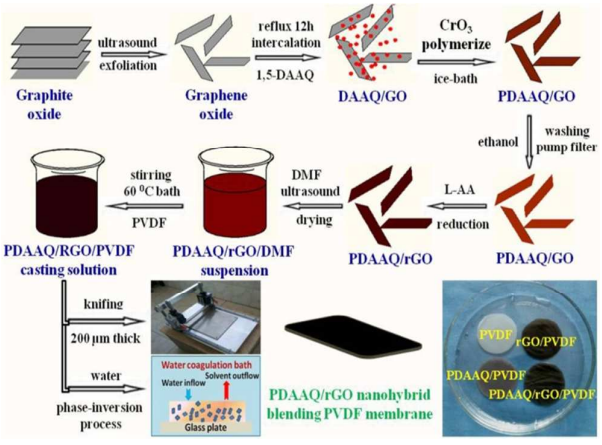

Figure 1 The schematic illustration about the preparation process of PDAAQ/rGO nanohybrid blended PVDF membranes.

2.5 Permeation and antifouling properties of membranes

The water permeability, BSA rejection and flux recovery of various membrane were conducted on a self-made dead-end stirred cell filtration system at a constant trans-membrane pressure of 0.25 MPa and 25 ± 2 ^{0}C. The effective membrane area was 34.2 cm^2 and 0.5 g L^{-1} BSA solution in PBS (pH 7.4) was used for rejection experiment. Each of the membrane was pre-compacted under 0.25 MPa trans-membrane pressure for 1 h to measure the stable pure water flux J_W (L m^{-2} h^{-1}), then pure water was replaced by 0.5 g L^{-1} BSA solution at the same trans-membrane pressure for 1 h, and the permeate flux was recorded as J_P (L m^{-2} h^{-1}). After filtrating feed solution, the membrane was hydraulically cleaned with distilled water for three times or electrically cleaned for 2 h on a DJS292-RS232 double constant potentiostat/galvanostat (shanghai) by scanning cell voltage of 1.0 V in air-aearted pH 7.4 PBS solution. The anode was a stainless steel mesh (25 cm^2) with 1 cm distance to the conductive membrane. Then, the recovered water flux was re-evaluated and expressed as J_{WC}. BSA concentration in the permeation and feed solution were measured by an UV-spectrophotometer (techcomp UV-1000, China) at 280 nm. The permeation fluxes (J_W) and BSA rejection (R) were calculated by following equations, respectively.[18]

$$J_W = \frac{V}{A \cdot \Delta t} \quad (1)$$

$$R\,(\%) = (1 - \frac{C_P}{C_F}) \times 100 \quad (2)$$

where V (L) is the volume of permeated water, A (m^2) is the membrane effective area, Δt (h) is the permeation time; C_P and C_F are BSA concentration of permeation and feed solution, respectively. C_F was maintained at 0.5 g L^{-1}, while C_P was sampled in permeation solution after 1 h BSA ultrafiltration. In order to evaluate the antifouling ability of the membranes, the

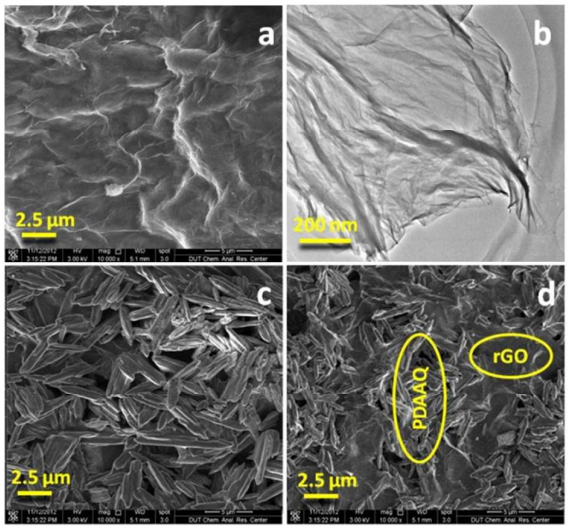

Figure 2 SEM images of **(a)** GO, **(b)** PDAAQ, **(c)** PDAAQ/rGO nanohybrid and TEM image of GO **(b)**.

flux recovery ratio (FRR) were defined and calculated by equation (3):

$$\mathrm{FRR}(\%) = \frac{J_{\mathrm{WC}}}{J_{\mathrm{W}}} \times 100 \quad (3)$$

The fouling-resistant capacity of membrane was further quantified with the total fouling ratio (R_t), reversible fouling ratio (R_r) and irreversible fouling ratio (R_{ir}), which were defined and calculated respectively as follows:[18]

$$R_{\mathrm{t}}(\%) = (1 - \frac{J_{\mathrm{p}}}{J_{\mathrm{w}}}) \times 100 \quad (4)$$

$$R_{\mathrm{r}}(\%) = \frac{J_{\mathrm{WC}} - J_{\mathrm{P}}}{J_{\mathrm{W}}} \times 100 \quad (5)$$

$$R_{\mathrm{ir}}(\%) = \frac{J_{\mathrm{W}} - J_{\mathrm{WC}}}{J_{\mathrm{W}}} \times 100 \quad (6)$$

In order to evaluate the antifouling performance of the conductive PDAAQ/rGO nanohybrid blended PVDF membrane, the continuous-flow filtration tests were conducted for three cycles to compare the filtration behaviours with and without external electric field of 1.0 V/cm (each cycle used a new membrane and lasted for 3.0 h). The anodes were two pieces of stainless steel mesh that were placed at both sides of the membrane module with 1.0 cm distance to the conductive PDAAQ/rGO/PVDF membrane cathode. A quartz sand aerator was fixed below the membrane module to supply air for in-situ H_2O_2 electro-generation and to maintain a cross-flow velocity along membrane surface.

3. Results and discussion

3.1 Characterization of PDAAQ/rGO nanohybrid

The preparation of PDAAQ/rGO nanohybrid blended PVDF membrane mainly involved two steps: synthesis of PDAAQ/rGO nanohybrid and immerged phase-inversion process. Characterization methods of SEM, TEM and XPS were used to confirm the successful synthesis of the PDAAQ/rGO samples. As shown in **Figure 2a** and **b**, the SEM and TEM images of GO exhibit the thin wrinkled laminar surface with a randomly aggregated worm-like structure, confirming the exfoliation of graphite oxide and the existing of graphene nanosheets in GO. The SEM images of PDAAQ and PDAAQ/rGO samples shown in **Figure 2c and d** obviously reveal a barleycorn-like morphology and pore structure of PDAAQ, while this irregular barleycorn-like morphology is freely stacking upon the uniform two-dimensional graphene layers for PDAAQ/rGO sample, indicating the successful PDAAQ modification of rGO surface. This can be further confirmed by the XPS spectra for qualitative analysis of C, N and O elements.

Figure 3 illustrates the typical C1s XPS curve-fitting spectra of GO and PDAAQ/rGO. The wide-scan XPS spectra of GO and PDAAQ/rGO shown in the inset of Figure 3 display the presence of only carbon and oxygen atoms for GO material, while a new peak corresponding to N 1s appears at approximate

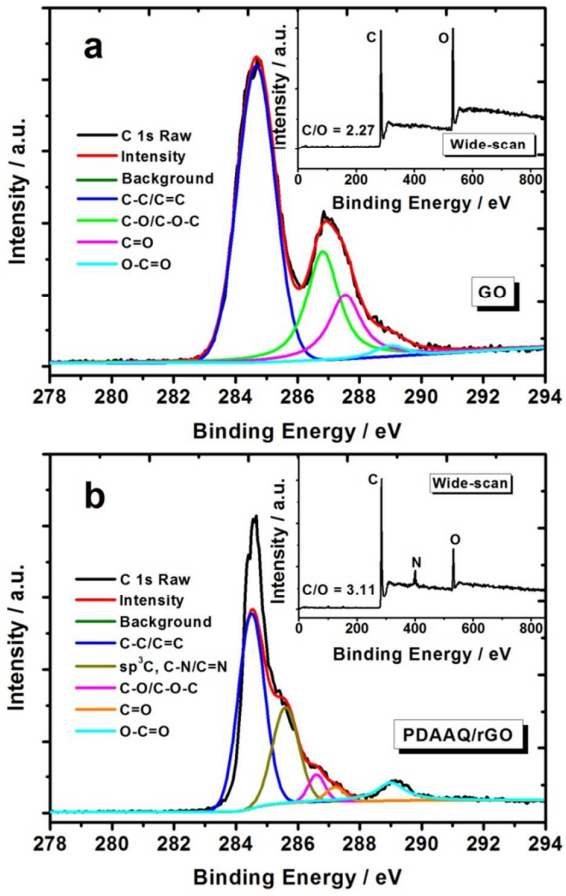

Figure 3 Core-level high-resolution C 1s XPS spectra of **(a)** GO and **(b)** PDAAQ/rGO. The inset shows the corresponding XPS wide-scan spectrum.

402 eV for PDAAQ/rGO sample, which is attributed to the amido groups of PDAAQ.[46] The C/O ratio of GO and PDAAQ/rGO measured by the ratio of C 1s to O 1s peak areas increases clearly from 2.27 to 3.11, indicating the efficient elimination of most oxygen-containing functional groups of GO after chemical reduction by L-AA. More importantly, the decreased oxygen content accordingly increases the number of sp^2 carbons on rGO nanosheet surfaces, resulting in an increase in π–π interaction between rGO and PDAAQ chains, which can significantly facilitate the electron-transfer and bring a synergistic effect to the electrochemical performances of the PDAAQ/rGO nanohybrids.[46,48] Additionally, the C1s peaks of GO (Figure 3a) can be deconvoluted into four components that centered at about 284.4, 286.6, 287.5, and 289.2 eV, corresponding to carbon atoms in different functional groups: C–C/C=C (sp^2 C), C–O–C (hydroxyl and epoxy), C=O (carbonyl) and O–C=O (carboxyl) oxygen-containing functional groups, respectively.[20,46] While for PDAAQ/rGO (Figure 3b), an apparent new peak at ca. 285.8 eV was obtained besides other four peaks that observed in C 1s spectrum of GO, which is assigned to C–N/C=N groups.[20] According to above SEM, TEM and XPS characterization data, the proposed chemical oxidative polymerization-reduction method is an effective strategy for synthesizing PDAAQ/rGO nanohybrid.

3.2 Characterization of PDAAQ/rGO/PVDF membranes

It can be observed from Figure 1 that the pristine PVDF and PDAAQ/PVDF membranes exhibit white and dark-gray color, respectively. After modified by rGO, the black rGO/PVDF and PDAAQ/rGO/PVDF membranes were obtained. To confirm the successful modification of PVDF membrane, the FTIR-ATR spectra of pristine PVDF, rGO/PVDF, PDAAQ/PVDF and PDAAQ/rGO/PVDF membranes were measured for qualitative analysis of surface functional groups. The most prominent feature of pristine PVDF spectrum shown in **Figure 4** is the sharp and intense peaks at around 1403, 1170, 880 and 840 cm^{-1}, which can be assigned to the asymmetric stretching and deformation vibrations of C-H and the C-F stretching vibration of PVDF, respectively.[8,17,22] Also, the band at 840 cm^{-1} is ascribed to a mixed mode of CH_2 rocking and CF_2 asymmetric stretching vibration.[24] The absorption peaks at 3020 and 2980 cm^{-1} can be attributed to the CH_2 asymmetric and symmetric vibration.[8,22] These characteristic absorption peaks are retained well in other three spectra. In comparison to the pristine PVDF membrane, a wider peak at around 3440-3500 cm^{-1} is observed in rGO/PVDF, PDAAQ/PVDF and PDAAQ/rGO/PVDF samples, which suggests that almost all of the free -NH_2 groups in the DAAQ monomer took part in the polymerization process and changed to -NH- groups.[46,48] On the other hand, this absorption peak corresponds also to the hydroxyl groups of rGO, implying the incomplete reduction of GO and the improved surface hydrophilicity of the PDAAQ/rGO/PVDF membrane.

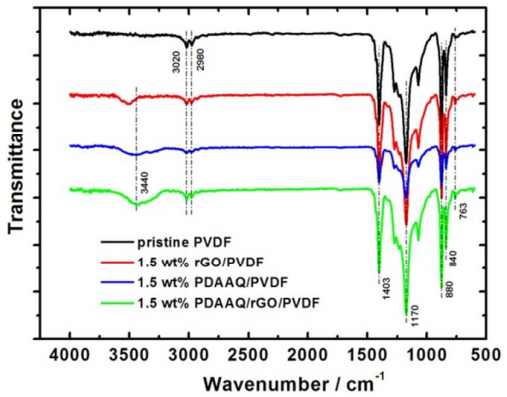

Figure 4 FTIR-ATR spectra of the pristine PVDF, rGO/PVDF, PDAAQ/PVDF and PDAAQ/rGO/PVDF membranes.

The surface morphologies of the pristine and blended PVDF membranes were characterized by FE-SEM (**Figure 5 a1-d1**). Unlike many other inorganic nanoparticles blended membrane,[14,15] no cracks and additives agglomeration are observed on these membrane surfaces, which indicates that the additives used are homogeneously dispersed on the PVDF membrane surface or membrane pores during the phase-inversion process. The three-dimensional AFM images of membranes are shown in **Figure 5 a2-d2** and the mean surface roughness (R_a) was calculated using the AFM analysis software in an AFM scanning area of 5 μm × 5 μm. Compared to the pristine PVDF membrane, three blended membranes present the obvious ridge- and valley-surface texture. The R_a value is increased by ca. 56%, 81% and 99% for rGO, PDAAQ and PDAAQ/rGO blended membranes, respectively. The chained PDAAQ effectively prevents the stacking and aggregation of the individual two-dimensional rGO nanosheets, which causes the PDAAQ/rGO blended membrane owning the biggest roughness. For a hydrophilic surface, wetting follows Wenzel's

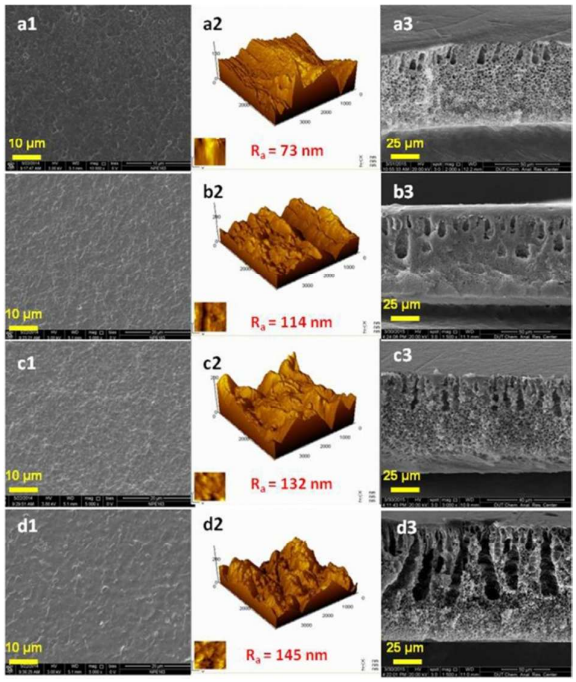

Figure 5 Membrane surface (**a1-d1**) and cross-section (**a3-d3**) SEM images and surface AFM images (**a2-d2**) of the pristine PVDF, rGO/PVDF, PDAAQ/PVDF and PDAAQ/rGO/PVDF membranes. All the additive proportion is 1.5 wt% based on the weight of PVDF.

model[49] and greater roughness leads to greater apparent hydrophilicity. Undoubtedly, the increased roughness provides more surface area for foulants to facilely accumulate in the valleys and thus compromise fouling resistance of a membrane. However, Xu et al.[17-19] has confirmed that higher membrane-surface roughness neither have any effect on the surface energy of the material itself, nor it cause a negative effect on membrane performance, and on the contrary, membrane hydrophilicity would be remarkably enhanced due to the increased surface area and the formation of cavities, which in turn controls the permeating flux and fouling resistance of membranes. This result is in accordance with trends in membrane permeability and separation performance depicted in the later part. To further explore the effect of additives on membrane microstructure, the cross-section SEM images of the pristine PVDF and blended membrane are surveyed and the results are presented in **Figure 5 a3-d3**. It can be seen that all the membranes show a typical asymmetric porous structure characterized by a skin layer, a much thicker finger-like porous substructure and a spongy-like bottom support. Compared to the pristine PVDF membrane, the thickness of blended membrane increases slightly and the finger-like pore structure develops obviously into much wider and thicker status. These results indicate that nano-scale additives play an important role in membrane microstructure adjustment.[18]

The porosity and mean pore size of various PVDF membranes are given in **Table 1.** It is clear that both porosity and mean pore size of the blended PVDF membranes are increased. This can be ascribed to the presence of PDAAQ and the incompletely reduced GO, which accelerates the diffusion and exchange rate between gels (water) and solvent (DMF) during the phase separation process.[17,50] The porosity of the blended membranes was in a range of 70–77%, which would undoubtedly play a positive role on promoting membrane permeability. On the other hand, increasing PDAAQ/rGO nanohybrid concentration leads to an obvious increase in porosity and mean pore size, while this trend cease when the quantity of PDAAQ/rGO additive reaches at 2.0 wt%, due to the pore blocking caused by the agglomeration of PDAAQ/rGO nanohybrids in high concentration.

3.3 Membrane hydrophilicity, Permeation flux and BSA rejection

Water contact angle is also presented in **Table 1** to evaluate the relative surface hydrophilicity of different PVDF membranes. In general, a low contact angle corresponds to a more hydrophilic membrane material.[8,51] An obvious decrease in the contact angle is observed for the blended PVDF membranes. The contact angle of 1.5 wt% rGO and PDAAQ blended PVDF membranes decreases respectively to 77.6 ± 2.1^0 and 74.7 ± 1.9^0 compared to 82.3 ± 2.3^0 of the pristine PVDF membrane, owing to the remnant oxygen-bearing –OH and –COOH groups on rGO, and N–H and C=O functional groups on PDAAQ. When 1.5 wt% PDAAQ/rGO nanohybrid was added to PVDF matrix, the contact angle reduces continuously and achieves the minimum value of 69.8 ± 1.3^0, which represents the highest hydrophilicity. This result is in accordance with the fact that the contact angle of a hydrophilic surface decreases with the increasing roughness.[18] Thus, the improved hydrophilicity will exert a favorable effect on the enhancement in the permeating flux and antifouling property of PDAAQ/rGO/PVDF membrane.

Table 1 Contact angle and pore structure parameters of vario us PVDF membranes.

membranea	mean pore size (nm)	porosity (%)	contact angle (deg)
pristine PVDF	8.2±0.1	65.0±1.3	82.3±2.3
1.5 wt% rGO/PVDF	9.1±0.4	70.5±2. 3	77.6±2.1
1.5 wt% PDAAQ/PVDF	10.6±0.6	74.6±2.9	74.7±1.9
0.5 wt% PDAAQ/rGO/PVDF	9.9±0.5	72.5±1.7	71.4±3.1
1.0 wt% PDAAQ/rGO/PVDF	10.2±0.5	73.8±3.1	71.1±3.6
1.5 wt% PDAAQ/rGO/PVDF	10.9±0.2	76.7±1.47	69.8±1.3
2.0 wt% PDAAQ/rGO/PVDF	9.8±0.4	72.2±1.92	72.2±2.9

Solute separation and solvent permeation are the two fundamental and essential properties of a membrane,[8,9] which are evaluated in present work by pure water flux (J_W) and BSA rejection measurement at the pressure of 0.25 MPa, respectively. It is clear from **Figure 6** that the water flux of blended membranes exhibits a similar trend to the pore structure and hydrophilicity that displayed in Table 1, indicating that the combined effect of pore size/porosity and hydrophilicity is responsible for the improvement in water flux.[19,51] In this regard, (i) the hydrophilicity of PDAAQ/rGO blended membranes increases with increasing PDAAQ/rGO content up to 1.5 wt%. The uniformly dispersed PDAAQ/rGO in the casting solution would attract water molecules inside the

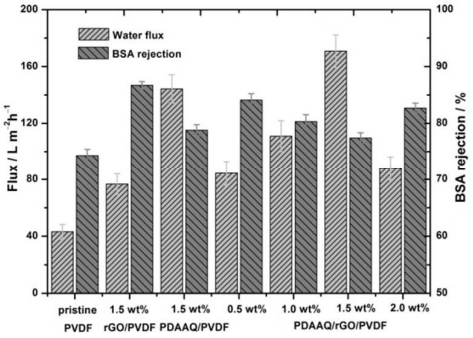

Figure 6 Effects of additive type and content on pure water flux and BSA rejection of various PVDF membranes at 0.25 MPa.

membrane matrix and facilitated their permeation through the membrane; (ii) adding hydrophilic PDAAQ/rGO nanohybrids into PVDF would promote the diffusion of DMF from polymer matrix into water. It is just the rapid phase demixing between solvent and non-solvent resulting in large pore formation and high porosity, thus promoting the transportation of water.[17,18] Therefore, it can be safely concluded that the increased hydrophilicity and enlarged pore size account for the improvement in pure water flux of membranes.

The results of BSA rejection by different PVDF membrane are also depicted in Figure 6. As seen, a ca.74.3% BSA rejection rate is observed, indicating the deposition and adsorption of a large amount of BSA on the pristine and hydrophobic PVDF membrane surface. While the BSA rejection distinctly increases for all the blended membranes, which is due mainly to the decreased hydrophobic interaction between hydrophilic/dense membrane surface and BSA protein solution, leading to the different degree of growth in solvent permeation and BSA rejection.[17,52] Additionally, it is worth noting that the BSA rejection of PDAAQ/rGO blended membranes displays a contrary trend in comparison to the water flux tendency. A slight decrease in BSA rejection is observed for 1.5 wt% PDAAQ/rGO blended membrane (77.4%) when compared with that for other three PDAAQ/rGO/PVDF membranes. This phenomenon can be attributed to the greater hydrophilicity and the larger pore size, which not only reduces water permeation resistance but also gives BSA molecules more opportunity to penetrate through larger membrane pores.[17,18,53,54] Consequently, the permeability and selectivity of membranes are mainly regulated by the superior hydrophilicity and the appropriate pore size/porosity. In terms of the results shown in Figure 6 and Table 1, it is clear that 1.5 wt% PDAAQ/rGO blended PVDF membrane exhibits ideal performance.

3.4 Antifouling properties of membranes during BSA filtration

In order to investigate the antifouling properties of the pristine and blended PVDF membranes, the dynamic filtration tests were conducted using BSA in PBS (pH 7.4) as a model protein. Filtration measurements are designed into three stages. To effectively lower the concentration polarization, the trans-membrane pressure and stirring speed were maintained at 0.25 MPa and 350 rpm,[17,55] respectively, during the whole filtration process. The first stage is 30 min pure water permeation. The second stage is 1 h ultrafiltration of BSA solution and the third stage is the pure water flux of the cleaned membranes by tap-water scrubbing, aeration scouring (aeration, 0 V/cm) and electric cleaning (aeration, 1.0 V/cm) for another 30 min. The typical time-dependent permeation flux of membranes is depicted in **Figure 7a, c and e**. It can be clearly found that the initial water flux for 1.5 wt% rGO, PDAAQ and PDAAQ/rGO blended PVDF membranes are much higher than that of the pristine PVDF membrane. In comparison, the permeation flux of BSA solution undergoes a dramatic decline for all membranes, owing to the adsorption or deposition of protein molecules on membrane pore wall or surface, which narrows pore size and causes membrane fouling.[9,12,17,51]

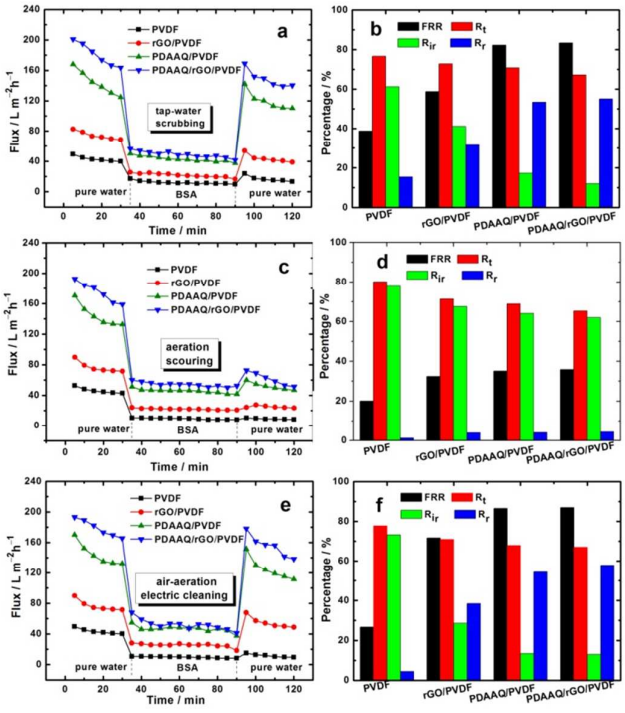

Figure 7 The antifouling properties of membranes. **(a), (c)** and **(e)** Time-dependent permeation flux of different membranes at 0.25 MPa during three steps: water flux for 30 min, BSA solution flux for 60 min, and water flux for 30 min after tap-water scrubbing, aeration scouring and electric cleaning, respectively; **(b), (d)** and **(f)** water flux recovery and fouling resistance ratio of various membranes.

It is clear from the third stage that the pure water flux can be recovered in different degrees, but not completely reverted after membranes hydraulic and electrical cleaning, due to the entrapment of proteins within the pores. Nevertheless, the FRR of all blended membranes is always higher than that of the pristine membrane under the same operating conditions, indicating that the blended membranes possess a more favourable antifouling performance.[17,22] Additionally, an interesting and meaningful finding is that the water flux of all the blended membranes can also be drastically resumed as well as the tap-water scrubbed membrane, after electrical cleaning. This result suggested that the external electric field and aeration scouring play a significant role on membrane fouling mitigation.

To quantitatively investigate the antifouling property during BSA protein filtration, the R_t, R_r, R_{ir} and FRR of the hydraulically and electrically cleaned membranes are calculated and summarized in **Figure 7 b, d and f**, respectively.

(i) Hydraulically cleaned membrane: The FRR values of tap-water scrubbed pristine PVDF membranes are only 38.9%, while approximately 71.7%, 82.5% and 86.8% of FRR values are obtained for 1.5 wt% rGO, PDAAQ and PDAAQ/rGO blended PVDF membranes, respectively, which accords with the hydrophilicity trend of membranes (Table 1) and implies the obvious enhancement in antifouling property. The excellent antifouling performance of the blended membranes can be attributed to the oxygen-containing functional groups of rGO and PDAAQ, which leads to a decrease in contact angle (Table

1) and an increase in membrane hydrophilicity. It is widely accepted that the higher hydrophilicity would generate a hydration layer on membrane surface, which can effectively eliminate deposited foulants and promote water molecule adsorption within the membrane during the hydraulic scrubbing.[17-19,51,56] In comparison, much lower FRR values were obtained for aeration scoured membranes, suggesting that the shear stress induced by aeration is inferior to tap-water scrubbing for removing the deposited foulants.

Generally, organic matter surface deposition or entrapping into pore (irreversible resistance, R_{ir}) and incompact adsorption on membrane surface (reversible resistance, R_r) are responsible for membrane fouling.[51] In present work, the R_{ir} values of tap-water scrubbed and aeration scoured pristine PVDF membrane was 61.3% and 77.9% (ca. 76.7% and 80.2% in total fouling, R_t), respectively, which demonstrates that the permeability of the pristine PVDF membrane is mainly influenced by physically irreversible fouling.[19,22] However, the irreversible fouling percentage of R_{ir} declines dramatically for tap-water scrubbed 1.5 wt% rGO/PVDF, PDAAQ/PVDF and PDAAQ/rGO/PVDF membranes, implying the superior antifouling and flux recovery properties. This should be ascribed to the increased surface roughness and hydrophilicity of the blended membranes.[8,9] Previous studies done by Xu et al.[17-19] confirmed that for hydrophilic membranes, a higher surface roughness can significantly improve membrane hydrophilicity and antifouling property when keeping all the other characteristics unchanged. It is evident that tap-water scrubbing can effective dislodge membrane fouling and restore the permeation flux, while the simple aeration scouring cannot achieve satisfactory fouling elimination.

(ii) Electrically cleaned membrane: By being remained under 1.0 V/cm external electrical field in air-aerated pH 7.4 PBS solutions for 2 h, the trends of FRR and fouling resistance are in line with those of the tap-water scrubbed membrane. It is clear that electric cleaning does not bring an improvement in FRR of the pristine PVDF membrane due to the innate insulating characteristic. Previously reports demonstrated that membrane hydrophilicity, pore structure, surface roughness and surface charge property affect the membrane fouling process, and naturally, the hydrophobic effect, hydrogen bonding, van der Waals forces and electrostatic force in turn control the tendency and degree of membrane fouling.[17,57] In this study, the BSA in PBS solution is negatively charged (the isoelectric point is ca. 4.78 and Zeta potential is ca. –24.4 mV), thus the electrostatic repulsive force can spontaneously repel the negatively charged BSA protein molecules away from the membrane surface, and as a result, enhancing the flux recovery effect.[36,38,44,45]

Compared to the PDAAQ and PDAAQ/rGO blended membrane, a larger R_{ir} is observed for rGO/PVDF membrane, which may be caused by its relatively low pore size/porosity and hydrophilicity. In terms of time-dependent permeability and FRR, electric cleaning is an effective approach in mitigating membrane fouling and 1.5 wt% PDAAQ/rGO nanohybrid blended PVDF membrane exhibits the highest FRR after electrical cleaning. Three factors might contribute to

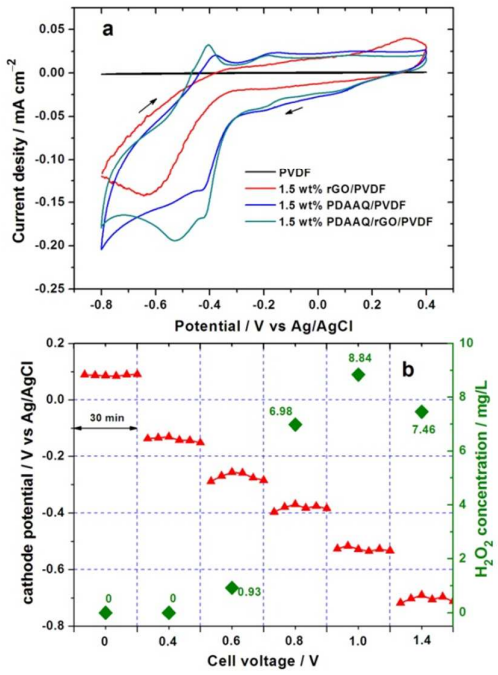

Figure 8 (a) Cyclic voltammograms of the prinstine and blended PVDF membrane in air-aerated pH 7.4 PBS solution at scan rate of 20 mV s^{-1}, **(b)** the relationship between cell voltage and cathode potential as well as the concentration of accumulated H_2O_2 for 1.5 wt% PDAAQ/rGO nanohybrid blended PVDF membrane after 30 min electrolysis.

this incremental fouling mitigation. Besides abovementioned electrostatic repulsive force and aeration scouring shear stress, the other important factor should be related to the generation of H_2O_2 on the PDAAQ/rGO/PVDF membrane. To explore the electrocatalytic activity of different fresh membranes towards ORR and in-situ H_2O_2 generation, the cyclic voltammograms are recorded in air-aerated pH 7.4 PBS solutions and the results are shown in **Figure 8a**. As seen, a larger cathodic peak current and a more positive peak potential at ca. –0.53 is clearly observed for PDAAQ/rGO/PVDF membrane. Compared to PDAAQ/PVDF membrane, the introduction of rGO markedly increases the electron-transport rate between quinine/hydroquinone (Q/HQ) redox couple and dissolved oxygen molecules, hence endowing PDAAQ/rGO/PVDF membrane a more superior electrocatalytic activity towards ORR.[46] The relationship between cathode potential and cell voltage for 1.5 wt% PDAAQ/rGO/PVDF membrane is displayed in **Figure 8b**. It is clear that the cathode potential (vs. 1.0 mol L^{-1} Ag/AgCl) becomes more negative (0.088 to –0.705 V) with increasing cell voltage from 0 to 1.4 V. The average cathode potential of ca. –0.522±0.012 V is obtained when cell voltage reaches at 1.0 V and a highest concentration of electrogenerated H_2O_2 at ca. 8.84 mg L^{-1} is achieved accordingly after 30 min electrolysis, suggesting that 1.0 V cell voltage can ensure the highest electro-activity towards the in-situ electro-generation of H_2O_2. Moreover, it is reported that the amino acid side chains of protein molecules can be directly oxidized into carbonyl groups by the active oxygen species such as $HO^{\bullet}$, $O_2^{\bullet-}$, $^1O_2$ and H_2O_2 as well as repulsive force

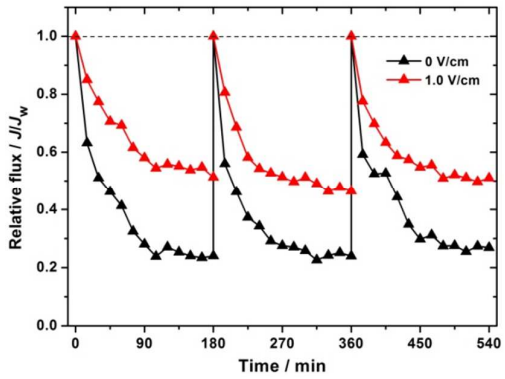

Figure 9 Changes of relative fluxes using BSA in PBS (pH 7.4) as model foulant with and without an external electric field.

between BSA protein molecules and cathodic membrane.[45,51] In combination with FRR analysis in Figure 7, it can be concluded that the improvement in repulsive force induced by an external electric field and H_2O_2 electro-generation is the predominant fouling reduction mechanism for PDAAQ/rGO/PVDF membrane. Hence, the fouling elimination in this study is closely related to the effect of cathode material and the corresponding cathode potential.

To further explore the antifouling performance of PDAAQ/rGO/PVDF membrane with an external electric filed, the continues-flow BSA filtration tests was conducted and compared with the control test without an external electric field. The time-dependent relative flux (J/J_w) changes of BSA are depicted in **Figure 9**. As seen, a much lower decay rate in J/J_w (average ca. 46.6%) is obviously observed for the conductive PDAAQ/rGO/PVDF membrane with 1.0 V/cm external electric field compared to the control test (average ca. 73.4%) under the same conditions. This demonstrates that in the presence of an external electric field, the air-aeration continues-flow filtration process which induces the combination of cross-flow shear stress and increased electrostatic repulsive force results in a ca. 63.5% increment in membrane fouling resistance.

The major mechanism for external electric field-promoted fouling mitigation can be schematically illustrated in **Figure 10**. Generally speaking, the best antifouling property towards BSA protein of the PDAAQ/rGO/PVDF membrane can be related to the improved hydrophilicity, pore size/porosity and surface roughness of the membrane. High surface roughness can improve membrane hydrophilicity in some extent, which in turn decreases the hydrophobic adsorption between BSA protein and membrane surface, thus reducing membrane fouling.[8,17-19] Simultaneously, the increased pore size/porosity can accumulate water permeation flux.[42] On the other hand, the combination of cross-flow shear stress and the enhanced electrostatic repulsive force in the presence of external electric field and the in-situ electro-generated H_2O_2 attribute to the fouling mitigation in the electric cleaning and continuous-flow electrochemical membrane filtration process. Furthermore, the antifouling properties of 1.5 wt% PDAAQ/rGO nanohybrid blended PVDF membranes during the long-term operation in continuous-flow MBR under an external electric field are being

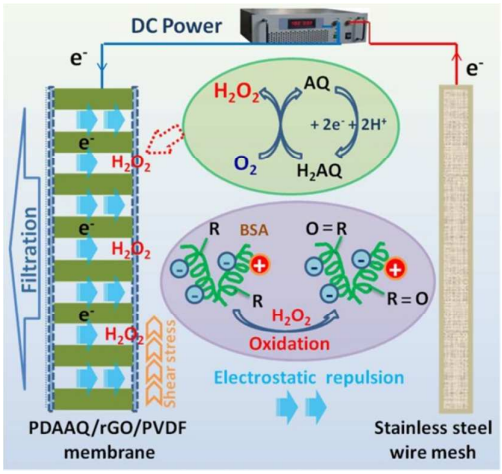

Figure 10 schematic illustration of electric cleaning and antifouling mechanisms of 1.5 wt% PDAAQ/rGO/PVDF membrane under external electric field.

studied in our laboratory. The potential impacts of external voltage on microbial activity, sludge mixed liquor property, concentrations of SMP and EPS are investigated and monitored at length to further elucidate the electrochemical antifouling mechanisms of the conductive PDAAQ/rGO/PVDF membrane.

4. Conclusions

In this work, a novel conductive PDAAQ/rGO/PVDF membrane was fabricated via the phase inversion process. The additives concentration plays a significant role on the characteristics of blended membranes. Among them, 1.5 wt% PDAAQ/rGO/PVDF membrane possesses the biggest pore size/porosity and the highest surface roughness, which greatly improve membrane hydrophilicity, permeability and BSA rejection compared with those of the pristine PVDF membrane. By applying an appropriate external electric field of 1.0 V/cm, the conductive PDAAQ/rGO nanohybrid blended PVDF membrane exhibits good electrocatalytic activity towards in-situ H_2O_2 generation and superior antifouling property along with higher flux recovery ratio and fouling resistance during the electric cleaning and continuous-flow electrochemical membrane filtration process. The cross-flow shear stress induced by aeration scouring and the increased electrostatic repulsion force induced by external electric field and the in-situ electro-generated H_2O_2 attribute to the fouling mitigation. The antifouling ability and mechanism of this conductive membrane during the long-term operation in continuous-flow MBR are being studied in depth by our research group to optimize operating conditions for its potential application in real wastewater treatment.

Acknowledgements

The authors acknowledge the financial support from the National Natural Science Foundation of China (no. 21437001, 21177017).

Notes and references

1 G.-D. Kang, and Y.-M. Cao, *J. Membr. Sci*., 2014, **463**, 145–165.
2 Z. W. Y. Sui, X. Gao, and C. Gao, *J. Membr. Sci*., 2012, **413-414**, 38–47.
3 F. Liu, N. A. Hashim. Y. Liu, M. R. M. Abed, and K. Li, *Fuel Energy Abstr*., 2011, **375**, 1–27.
4 J.-W. Lee, J.-Y. Jung, Y.-H. Cho, S.-K Yadav, K.-Y. Baek, H.-B. Park, S.-M. Hong, and C.-M. Koo, *ACS Appl. Mater. Interfaces* 2014, **6**, 14600–14607.
5 A. W. Zularisam, A. F. Ismail, and M. R. Salim, *Desalination* 2006, **194**, 211–231.
6 W. Gao, H. Liang, J. Ma, M. Han, Z. L. Chen, Z. S. Han, and G. B. Li, *Desalination* 2011, **272**, 1–8.
7 Z.-L. Xu, L.-Y. Yu, and L.-F. Han, *Front. Chem. Eng. China* 2009, **3**, 318–329.
8 A. Qin, X. Li, X. Zhao, D. Liu, and C. He, *ACS Appl. Mater. Interfaces*, 2015, **7**, 8427–8436.
9 M. Safarpour, A. Khataee, and V. Vatanpour, *Ind. Eng. Chem. Res*., 2014, **53**, 13370–13382.
10 S.-W. Meng, J. Mansouri, Y. Ye, and V. Chen, *J. Membr. Sci*., 2014, **450**, 48-59.
11 H. Chen, L. Kong, and Y. Wang, *J. Membr. Sci*., 2015, **487**, 109–116.
12 N. A. Hashim, Y. T. Liu, and K. Li, *Ind. Eng. Chem. Res*., 2011, **50**, 3035–3040.
13 S. Liang, Y. Kang, A. Tiraferri, E. P. Giannelis, and X. Huang, *ACS Appl. Mater. Interfaces*, 2013, **5**, 6694–6703.
14 H. Wu, J. Mansouri, and V. Chen, *J. Membr. Sci.*, 2013, **433**, 135–151.
15 Y. Lu, H. Sun, L. L. Meng, and S. L. Yu, *Sep. Purif. Technol.*, 2009, **66**, 347–352.
16 S. Liang, K. Xiao, Y. H. Mo, and X. Huang, *J. Membr. Sci*., 2012, **394-395**, 184–192.
17 T. Wu, B. Zhou, T. Zhu, J. Shi, Z. Xu, C. Hu, and J. Wang, *RSC Adv*., 2015, **5**, 7880–7889.
18 J. Zhang, Z. Xu, W. Mai, C. Min, B. Zhou, M. Shan, Y. Li, C. Yang, Z. Wang and X. Qian, *J. Mater. Chem. A*, 2013, **1**, 3101–3111.
19 J. Zhang, Z. Xu, M. Shan, B. Zhou, Y. Li, B. Li, J. Niu, and X. Qian, *J. Membr. Sci*., 2013, **448**, 81–92.
20 X. Chang, Z. Wang, S. Quan, Y. Xu, Z. Jiang, and L. Shao, *Appl. Surface Sci*., 2014, **316**, 537–548
21 H. M. Hegab, and L. Zou, *J. Membr. Sci*., 2015, **484**, 95–106.
22 C. Zhao, X. Xu, J. Chen, G. Wang, and F. Yang, *Desalination*, 2014, **340**, 59–66.
23 S. Bano, A. Mahmood, S.-J. Kim and K.-H. Lee, *J. Mater. Chem. A*, 2015, **3**, 2065–2071.
24 N.N. Li, C. F. Xiao, S. L. An, and X. Y. Hu, *Desalination*, 2010, **250**, 530–537.
25 N. Pezeshk, D. Rana, R. M. Narbaitz, and T. Matsuura, *J. Membr. Sci*., 2012, 389, 280–286.
26 A. Venault, Y.-H. Liu, J.-R. Wu, H.-S. Yang, Y. Chang, J.-Y. Lai, and P. Aimarc, J. *Membr. Sci*., 2014, **450**, 340–350.
27 Q. Y. Bi, Q. Li, Y. Tian, Y. K. Lin, and X. L. Wang, *J. Appl. Polym. Sci*., 2013, **127**, 394–401.
28 X. Huang, W. Wang, Y. Liu, H. Wang, Z. Zhang, W. Fan, and L. Li, *Chem. Eng. J*., 2015, **273**, 421–429.
29 C.-F. de Lannoy, Da. Jassby, K. Gloe, A. D. Gordon, and M. R. Wiesner, *Environ. Sci. Technol.*, 2013, **47**, 2760–2768.
30 M. Zhang, W. Peng, J. Chen, Y. He, L. Ding, A. Wang, H. Lin, H. Hong, Y. Zhang, and H. Yu, *Water Res*., 2013, **47**, 2777–2786.
31 A. V. Dudchenko, J. Rolf, K. Russell, W. Duan, and D. Jassby, *J. Membr. Sci*., 2014, **468**, 1–10.
32 L. Liu, F. Zhao, J. Liu, and F. Yang, *J. Membr. Sci*., 2013, **437**, 99–107.
33 W. Duan, A. Dudchenko, E. Mende, C. Flyer, X. Zhu, and D. Jassby, *Environ. Sci.: Processes Impacts* 2014, **16**, 1300–1308.
34 Z. Wang, J. Huang, C. Zhu, J. Ma, and Z. Wu, *Chem. Eng. Technol*., 2013, **36**, 2044–2050.
35 Y. Wang, W. Li, G. Sheng, B. Shi, and H. Yu, *Water Res*., 2013, **47**, 5794–5800.
36 L. Liu, J. Liu, B. Gao, F. Yang, and S. Chellam, *J. Membr. Sci.*, 2012, **394-395**, 202–208.
37 W. E. Price, C. O. Too, G. G. Wallace, and D. Zhou, *Synth. Met*., 1999, **102**, 1338–1341.
38 L. Liu, J. Liu, B. Gao, F. Yang, J. Crittenden, and Y. Chen, *J. Membr. Sci.*, 2013, **429**, 252–258.
39 J.-L. Ma, Y.-F. Zhao, Z.-W. Xu, C.-Y. Min, B.-M. Zhou, Y.-L. Li, B.-D. Li, and J.-R. Niu, *Desalination*, 2013, **320**, 1–9.
40 Q. Zhang, and C. D. Vecitis, *J. Membr. Sci*., 2014, **459**, 143–156.
41 C. F. deLannoy, D. Jassby, D. D. Davis, and M. R. Wiesner, *J. Membr. Sci*., 2012, **415-416**, 718–724.
42 G. Gao, Q. Zhang, Z. Hao, and D. Vecitis, *Environ. Sci. Technol.*, 2015, **49**, 2375–2383.
43 C. A. Crock, A. R. Rogensues, W. Shan, and V. V. Tarabara, *Water Res*., 2013, **47**, 3984–3996.
44 L. Xu, G. Zhang, G. Yuan, H. Liu, J. Liu, and F. Yang, *RSC Adv*., 2015, **5,** 22533–22543
45 J. Huang, Z. Wang, J. Zhang, X. Zhang, J. Ma, and Z. Wu, *Sci. Rep*., 2015, **5**, DOI:10.1038/srep09268.
46 H. Liu, G. Zhang, Y. Zhou, M. Gao, and F. Yang, *J. Mater. Chem. A*, 2013, **1**, 13902–13913
47 W. S. Hummers, and R. E. Offeman, *J. Am. Chem. Soc*., 1958, **80**, 1339–1339.
48 Q. Wu, Y. Q. Sun, H. Bai and G. Q. Shi, *Phys. Chem. Chem. Phys*., 2011, **13**, 11193–11198.
49 A. Marmur, *Langmuir* 2003, **19**, 8343–8348.
50 N. Pezeshk, D. Rana, R. Narbaitz and T. Matsuura, *J. Membr. Sci.*, 2012, **389**, 280–286.
51 Z. Wang, J. Ma, C. Y. Tang, K. Kimura, Q. Wang, and X. Han, *J. Membr. Sci*., 2014, **468**, 276–307.
52 M. Hashino, K. Hirami, T. Ishigami, Y. Ohmukai, T. Maruyama, N. Kubota and H. Matsuyama, *J. Membr. Sci*., 2011, **384**, 157–165.
53 Q. Yang, N. Adrus, F. Tomicki and M. Ulbricht, *J. Mater. Chem*., 2011, **21**, 2783–2811.
54 K.-J. Hwang and P.-Y. Sz, *J. Membr. Sci.*, 2011, **378**, 272–279.
55 L. Wang, Y.-l. Su, L. Zheng, W. Chen and Z. Jiang, *J. Membr. Sci*., 2009, **340**, 164–170.
56 S. Zinadini, A. A. Zinatizadeh, M. Rahimi, V. Vatanpour and H. Zangeneh, *J. Membr. Sci*., 2014, **453**, 292–301.
57 V. Vatanpour, S. S. Madaeni, R. Moradian, S. Zinadini and B. Astinchap, *J. Membr. Sci*., 2011, **375**, 284–294.